Estimation of Road Surface Roughness Using Airborne Synthetic Aperture Radar

Arun Babu[a], Stefan V. Baumgartner[a], Gerhard Krieger[a], Lucas Germano Rischioni[a]
[a] Microwaves and Radar Institute, German Aerospace Center (DLR), Wessling, Germany
Email: Arun.Babu@dlr.de

Abstract

Since road surface roughness is an important factor for road safety, periodic monitoring of the road surface roughness is a necessity. Compared to the widely used costly, time-consuming and labour-intensive road surface roughness estimation using measurement vehicles all over the country, the potential of airborne polarimetric SAR to remotely estimate the road surface roughness is investigated in this study. The analysis of the airborne X-band polarimetric SAR datasets acquired by DLR's F-SAR system over the Kaufbeuren and Braunschweig test sites revealed that the X-band airborne SAR datasets are sensitive to the road surface roughness. The road surface roughness results estimated using different models are discussed in this paper.

1 Introduction

The road surface roughness is one of the significant factors which affects road safety [1]. The road surface roughness has a direct influence on the friction between the road surface and the tyres which affect the skid resistance of the vehicle [2]. The undulated vertical profile of the road surface is responsible for providing friction between the road surface and the tyres [3]. The Root Mean Square (RMS) height (h_{rms}) of this undulated vertical profile is considered as a measure of the road surface roughness as in (1) [4].

$$h_{rms} = \sqrt{\frac{\sum_{i=1}^{n}\left(h_i - \bar{h}\right)^2}{n-1}} \qquad (1)$$

where h_i is the vertical height at location i and $\bar{h}$ represents the mean vertical height of the surface for n samples.
An optimal amount of skid resistance is required for performing safe acceleration and braking. Because of these reasons, the road surface roughness needs to be periodically monitored to ensure that the road surface roughness values are in the optimal range to provide sufficient friction [5]. Currently, the road surface roughness is measured using measurement vehicles. But, this process is expensive, labour intensive, time-consuming and it is done only approximately every four years over German autobahns.
Considering the importance of the road surface roughness parameter, it should be estimated more frequently, at least annually. This study focuses on estimating the road surface roughness using fully polarimetric airborne synthetic aperture radar (SAR) datasets. The use of airborne SAR can help to estimate the road surface roughness on a wide scale and it is not labour intensive and time consuming compared to the conventional methods.

2 Test sites and datasets

Roads with different surface roughness values are required for this study. For this purpose, two different test sites were identified. The first test site is the Kaufbeuren airfield in Bavaria, Germany. It is a former military airfield that includes the runway, taxiways and parking areas composed of different materials like asphalt, concrete, etc. The Google Earth image of the Kaufbeuren test site is shown in **Figure 1 (a)**. The zoomed view on the top left side of the image shows the concrete and asphalt sections on the runway. The zoomed view on the bottom right side of the image shows the parking area with cracks and potholes. The repair works done on the runway are also visible in the zoomed view.

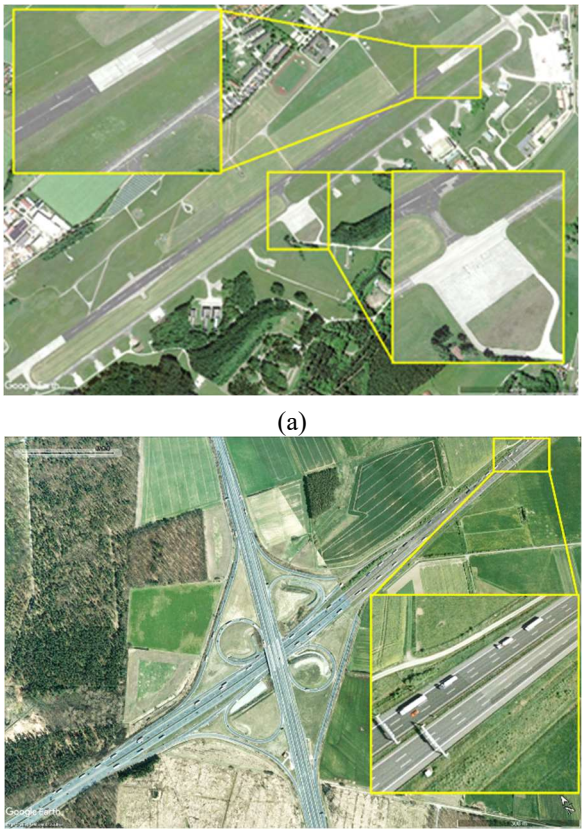

(a)

(b)

Figure 1 Google Earth images of the test sites used for this study. **(a)** Kaufbeuren test site, Bavaria. **(b)** Wolfsburg motorway intersection, Braunschweig.

The second test site is the Wolfsburg motorway intersection at Braunschweig, Germany. This test site is selected because of the long motorway without any disturbance from trees, buildings, etc. **Figure 1 (b)** shows the Google Earth image of this test site. Uniform surface roughness is expected at this test site. Towards the top right end of the image, it can be seen that there is a sudden change in the colour shade of the motorway. This may be due to repair work done at that region and a change in surface roughness can be expected there.

Fully polarimetric X-band airborne SAR datasets acquired over the Kaufbeuren and Braunschweig test sites with DLR's F-SAR system were used for this study. The details about the F-SAR datasets are given in **Table 1**.

Table 1 Characteristics of the F-SAR datasets

SAR system	F-SAR
Frequency band	X-band (9.60 GHz)
Polarimetric mode	Quad-pol
Look direction	Right
Spatial resolution	25 cm x 25 cm

The datasets were acquired over the Braunschweig test site on 31st August 2020, and over the Kaufbeuren test site on 4th September 2020. At each test site, several datasets were acquired from different directions (i.e., with different aspect angles) and also with different incidence angles.

Table 2 Ground truth surface roughness values

GT spot	Surface undulation (mm)		$GT\ h_{rms}$ (mm)	Remarks
	Min	Max		
1	-7.09	2.73	2.36	Repeated directional grooves
2	-3.00	2.27	0.99	Concrete, smooth
3	-2.53	1.70	0.66	Asphalt, smooth
4	-4.34	1.66	0.88	Maintenance work, smooth
5	-2.45	2.26	0.68	Asphalt, smooth
6	-4.14	2.01	0.98	Concrete, smooth
7	-3.03	2.62	1.09	Concrete, smooth
8	-2.38	1.91	0.61	Concrete, very smooth

A ground truth (GT) data collection activity was performed at the Kaufbeuren test site on 3rd September 2020 to measure the GT surface roughness values ($GT\ h_{rms}$). The GT data collection activity was performed just 1 day before the airborne SAR data acquisition to avoid any unexpected changes between the airborne SAR datasets and the GT data. The GT data were also acquired on a dry sunny day to prevent any measurement errors caused due to water filling the voids in concrete and asphalt surfaces. Eight GT spots with each of 1m^2 area were identified at the Kaufbeuren test site for the ground truth data collection. The GT spots were distributed over the runway, taxiway, and parking areas covering both smooth and rough regions made of concrete and asphalt. The $GT\ h_{rms}$ values were measured by laser scanning using a handheld laser scanner. The handheld laser scanner used for this purpose measured the vertical surface undulations of the road surface with a measurement resolution of 0.025 mm and also with an accuracy of 0.025 mm. **Table 1** shows the minimum-maximum surface undulations and the ground truth surface roughness values ($GT\ h_{rms}$) estimated at each of the ground truth spots. These $GT\ h_{rms}$ values can be used to validate the surface roughness values estimated using the airborne SAR datasets.

3 Methodology

From the SAR data, the remotely sensed parameter (ks) can be estimated which represents the effective vertical surface roughness. ks is a unitless parameter and the surface roughness (h_{rms}) can be estimated from the ks as follows [4]:

$$h_{rms} = \frac{ks}{(2\pi/\lambda_c)} \quad (2)$$

where λ_c is the centre frequency of the SAR system.

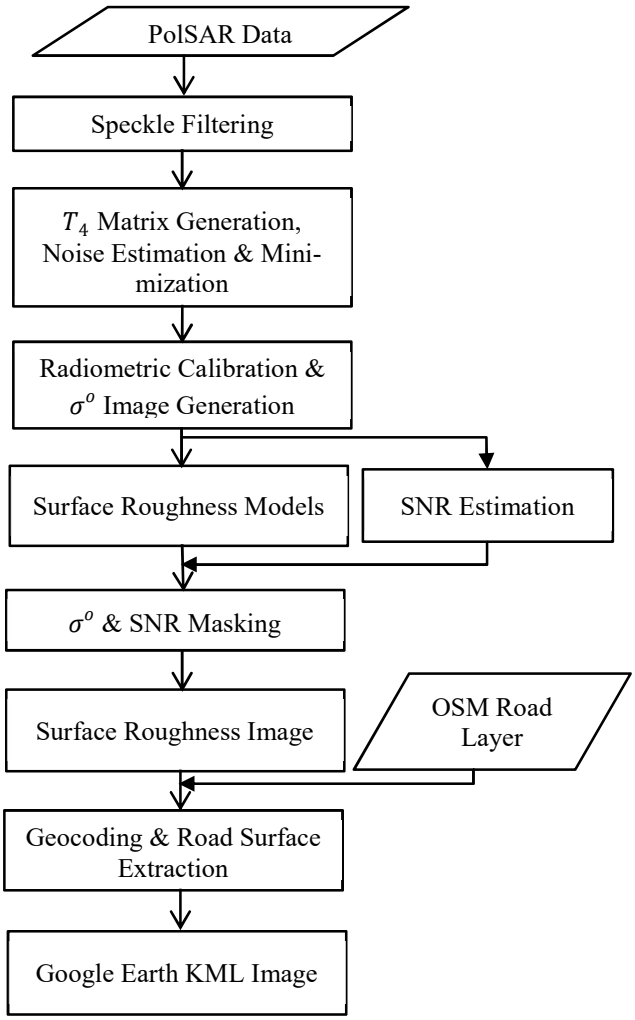

Figure 2 Block diagram of the processing scheme for road surface roughness estimation.

The block diagram to generate the surface roughness image

from the PolSAR dataset is shown in **Figure 2**. The airborne PolSAR dataset were first speckle filtered using a 3x3 Refined-Lee speckle filter [6]. After that, the speckle filtered PolSAR data was used to generate the 4x4 coherency matrix (T_4) [4]. The T_4 was estimated to carry out the additive noise estimation and minimization procedure. For this purpose, T_4 was diagonalized and the four eigenvalues were computed. The 4th eigenvalue (λ_4) represents the additive noise (N) present in the PolSAR data ($N = \lambda_4$). So, the additive noise can be minimized by subtracting the λ_4 from the first three eigenvalues of the T_4 matrix or by subtracting λ_4 from the diagonal elements of the 3x3 coherency matrix ($T_{3\ noise\ affected}$) [7]. After performing the additive noise estimation and minimization procedure, the radiometrically calibrated sigma nought (σ^o) images were generated for the co-polarization channels [8]. These σ^o images were used as the inputs for the road surface roughness estimation models.

3.1 Surface roughness estimation models

SAR backscatter-based and machine learning-based models were implemented in this study to investigate the capability of these models for road surface roughness estimation. The models implemented are listed in **Table 3**.
The SAR backscatter-based semi-empirical models utilize SAR backscatter values (σ^o) for the ks estimation.

Table 3 Surface roughness estimation models

SAR backscatter-based semi-empirical models	Machine learning-based models
Dubois model	Artificial Neural Network (ANN) regression
New semi-empirical model	Support vector regression
	Random Forest regression

The new semi-empirical model was developed based on the Dubois model [9]. According to the assumptions from the Dubois model, a radar signal in pq polarization can be written as a function of incidence angle, surface roughness, and surface moisture [10]. But, for a dry asphalt or concrete surface, the contribution from the surface moisture component to the radar signal is negligible. So, for the new model formulation, the radar signal can be written as a function of incidence angle and surface roughness after neglecting the surface moisture component. The relationship can be written as follows [11]:

$$\sigma_{pq}^o = \delta(\cos(\theta))^\beta\ (ks)^{\varepsilon \sin(\theta)} \quad (3)$$

In the above equation, σ_{pq}^o is the sigma nought backscatter value for the p transmitted and q received polarization. The term $\delta(\cos(\theta))^\beta$ denotes the relationship between σ_{pq}^o and the local incidence angle (θ). From this relationship, it can be understood that the σ_{pq}^o decreases as the incidence angle (θ) increases and this decrease in σ_{pq}^o is higher at low incidence angles and lower at high incidence angles. The second term $(ks)^{\varepsilon \sin(\theta)}$ indicates the relationship between σ_{pq}^o and the effective surface roughness (ks). σ_{pq}^o and ks have a power-law relationship and the sensitivity of σ_{pq}^o to ks is higher at high incidence angles than at low incidence angles. The $\sin(\theta)$ term is added to the relationship to minimize this incidence angle dependency. Equation (3) can be inverted to estimate ks as a function of σ_{pq}^o and incidence angle (θ) as follows:

$$ks = 10^{\left[\frac{\log(\sigma_{pq}^o) - \log(\delta(\cos(\theta))^\beta)}{\varepsilon\ sin(\theta)}\right]}. \quad (4)$$

In (4), $\delta, \beta,$ and ε are the unknown coefficients that need to be estimated to solve the equation. The coefficients can be estimated using the $GT\ h_{rms}$ values, σ_{pq}^o values and incidence angle values (θ) at the ground truth spots using the method of least square-based curve fitting.
The machine learning-based regression models used in this study also use the SAR backscatter values (σ^o) to estimate the road surface roughness values. The Artificial Neural Network (ANN) regression, support vector regression and random forest regression models were trained using the SAR training datasets and $GT\ h_{rms}$ values from the Kaufbeuren test site [12]. The trained models were then tested on the testing datasets from Kaufbeuren and Braunschweig test sites.

3.2 Sigma nought and SNR masking

High sigma nought values not corresponding to the road surface can cause errors in the road surface roughness estimation. The strong reflection from the lane dividers present in between the roads and also the strong reflection from the flyover walls cause invalid high surface roughness values which need to be eliminated. So, all the pixels with σ_{VV}^o greater than -10.96 dB were masked out from the final surface roughness image. This threshold is determined from the datasets.
Similar to the high sigma nought values not corresponding to the road surface, the very low signal-to-noise ratio (SNR) pixels can also result in unreliable surface roughness estimation. The surface roughness values of the regions where the SNR is less than the pre-determined minimum thresholds for each model are invalid and can be neglected to minimize the measurement biases/errors.

3.3 Geocoding and Google Earth visualization

To visualize the surface roughness images in Google Earth, the surface roughness images generated were geocoded from the slant-range coordinate system to a geographic coordinate system with a grid spacing of 0.25 m. The roads were then extracted from the surface roughness images with the help of the Open Street Map (OSM) road layer [13]. The OSMnx python package was used to download the road layers and all the surface roughness values outside the road layer were masked out from the final surface roughness image. Google Earth KML files were then generated which show the surface roughness results and the road boundaries. In this method, KML files representing surface roughness values of specific roads of interest can be generated by filtering using the type and names of the roads of interest. E.g., the filtering key "Motorway-A4" generates the surface roughness KML file for the motorway with the name A4.

4 Experimental results

The road surface roughness results obtained by processing the F-SAR datasets are discussed here.

Figure 3 (a) shows the surface roughness image of the Kaufbeuren test site estimated using the Dubois model. The surface roughness image is visualized in Google Earth after geocoding and masking out the regions outside the runway, taxiway, and parking areas. The near range and far range are marked in the image. Both ends of the runway are made of concrete and the middle region is made of asphalt. But in **Figure 3 (a)**, it can be observed that at the near range the Dubois model is unable to differentiate between concrete and asphalt. Both concrete and asphalt appear in blue indicating similar surface roughness. But, at the far range, the Dubois model can clearly distinguish between asphalt and concrete. The asphalt regions are appearing mainly in blue colour and the concrete regions are appearing in yellow and red colour. Also, a gradient increase in the surface roughness can be observed from near range to far range at the asphalt regions. All these observations point out that the surface roughness values estimated by the Dubois model are influenced by the incidence angle and the model sensitivity to surface roughness is less at the near range.

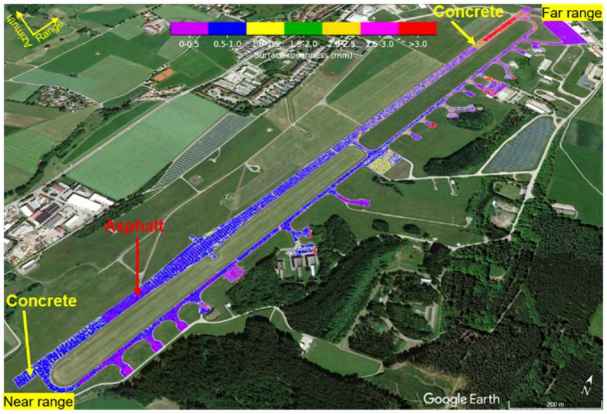

(a)

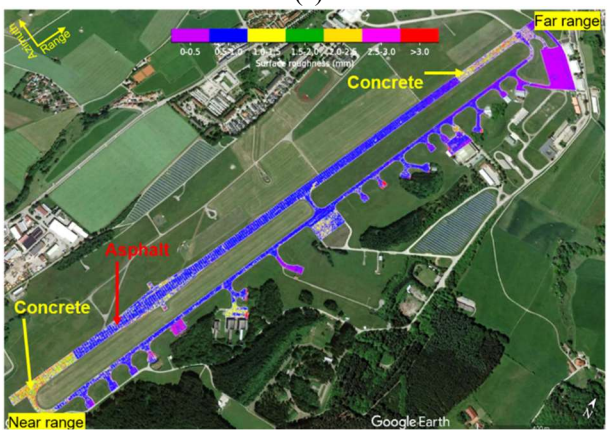

(b)

Figure 3 Surface roughness images of the Kaufbeuren test site. **(a)** Dubois model. **(b)** new model.

The new model is developed based on the Dubois model assumptions, with the aim to minimize this incidence angle dependency problem and also to improve the overall accuracy of the road surface roughness estimation. **Figure 3 (b)** shows the surface roughness image generated for the Kaufbeuren test site using the new model. By comparing **Figure 3 (b)** with the surface roughness image generated using the Dubois model shown in **Figure 3 (a)**, it can be seen that in the surface image generated from the new model, the concrete regions at both ends of the runway are showing a high value of surface roughness indicated by the yellow colour and the asphalt regions are showing a low value of surface roughness indicated by the blue colour. From this result, it can be clearly understood that the new model can distinguish between concrete and asphalt at both near range and far range which may also have different surface roughness. Also, if we look at the asphalt regions from near range to far range, it can be observed that the influence of incidence angle on surface roughness variations has reduced considerably.

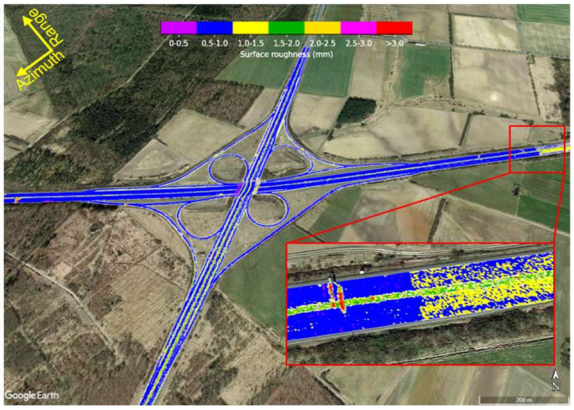

(a)

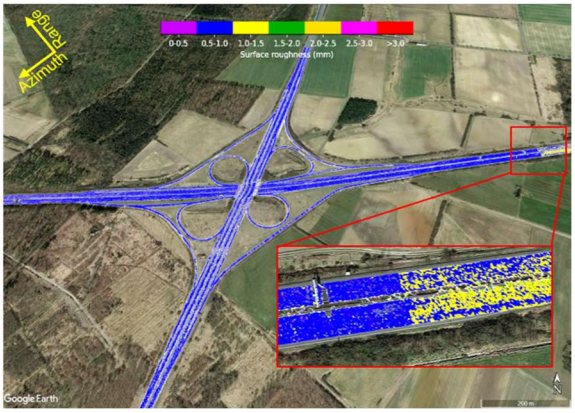

(b)

Figure 4 Surface roughness images of the Wolfsburg motorway intersection at Braunschweig. **(a)** without sigma nought and SNR masking. **(b)** with sigma nought and SNR masking.

Figure 4 (a) shows the surface roughness image generated using the new model for the Wolfsburg motorway intersection at Braunschweig, Germany, without performing sigma nought and SNR masking. The zoomed view in the figure shows a portion of the motorway where a change in surface roughness can be observed. This sudden change in surface roughness at the motorway may be due to maintenance work done in that region (cf. **Figure 1 (b)**). In the zoomed view, it can be seen that two red stripes are present across the road indicating high surface roughness values. These red stripes are caused due to the strong backscatter signal

from the overhead signboard present there and do not correspond to the actual surface roughness of that location. Also, the green colour present in between the two lanes of the motorway is caused due to the strong reflection from the lane dividers separating the two roads.

Figure 4 (b) shows the surface roughness image generated after performing both upper sigma nought threshold masking and lower SNR threshold masking. If we compare the zoomed view shown in **Figure 4 (b)** with the zoomed view shown in **Figure 4 (a)**, it can be observed that the two red stripes present in **Figure 4 (a)** due to the strong reflection from the signboards are not visible in **Figure 4 (b)** after upper sigma nought threshold masking. Also, it can be seen that the green colour present in between the lanes due to the reflection from the lane dividers is also removed. All the pixels with SNR less than 5.98 dB were masked out from the surface roughness image. By comparing **Figure 4 (b)** with **Figure 4 (a)**, it can be seen that some of the pixels corresponding to the blue colour got removed in **Figure 4 (b)**. These pixels were having an SNR of less than 5.98 dB. Both upper sigma nought threshold masking and low SNR threshold masking can be applied together to minimize the unreliable values from the surface roughness images.

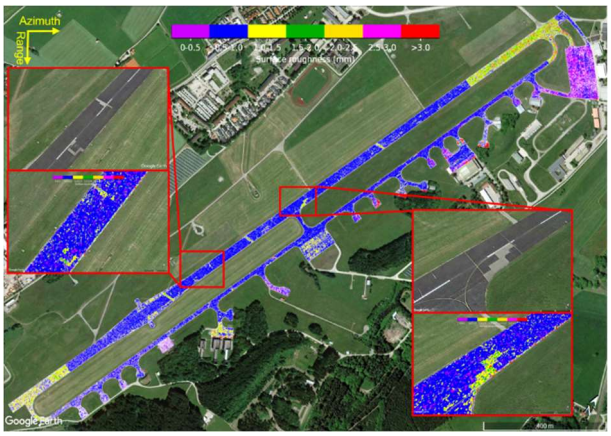

(a)

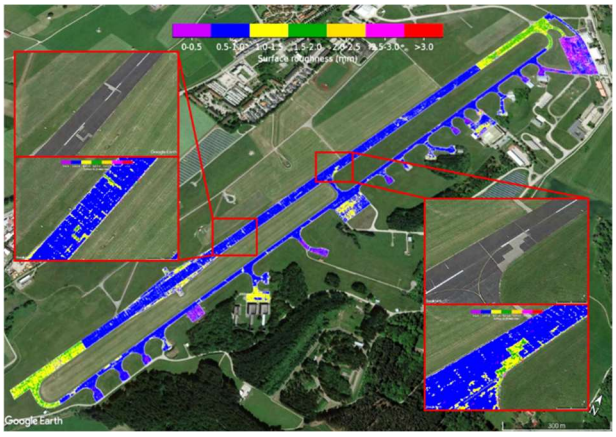

(b)

Figure 5 Surface roughness images of the Kaufbeuren test site. **(a)** surface roughness image generated using the new model. **(b)** single surface roughness image generated from multiple datasets using the multi-dataset averaging method.

The surface roughness images generated from a single dataset can contain unreliable surface roughness values caused due to shadow areas, speckle, low SNR regions, and incidence angle. To minimize these errors, the surface roughness images generated from multiple datasets having different acquisition geometries can be combined together using a multi-dataset averaging method to generate a single surface roughness image. In this method, a single surface roughness image is generated by performing pixel-wise averaging of the surface roughness results generated from multi-aspect angle datasets. The multi-dataset averaging is performed after upper sigma nought threshold masking and lower SNR threshold masking. **Figure 5 (a)** shows the surface roughness image generated using the new model and **Figure 5 (b)** shows the single surface roughness image generated from multiple datasets using the multi-dataset averaging method. By comparing both images, it can be seen that the multi-dataset averaging image looks much smoother compared to the other image. All the local variabilities present in **Figure 5 (a)** were smoothed out due to this multi-dataset averaging. From the zoomed view shown in **Figure 5 (b)**, it can be found that the result looks much better than the results shown in **Figure 5 (a)**. The repair works done on the runway can be seen in yellow colour and the surrounding regions are appearing in blue colour without many variations.

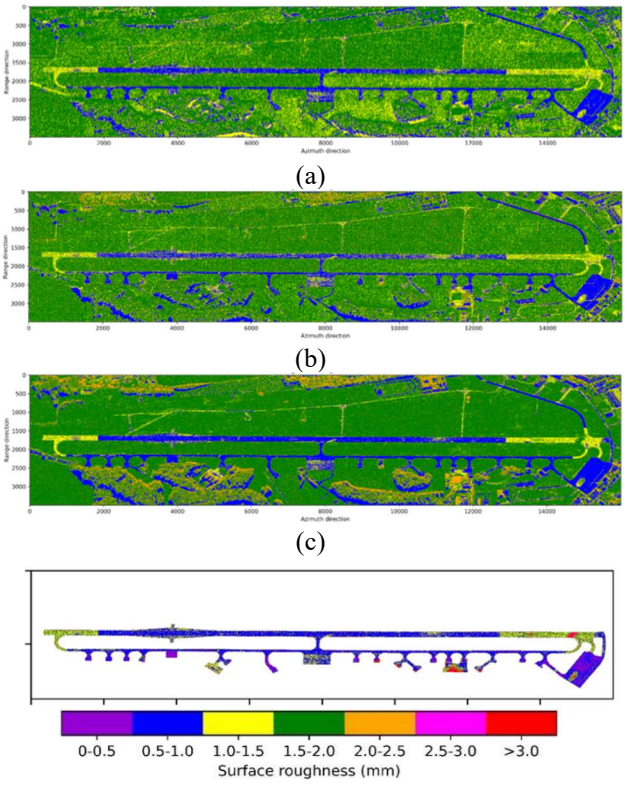

(a)

(b)

(c)

(d)

Figure 6 Surface roughness images of the Kaufbeuren test site. **(a)** support vector regression. **(b)** ANN regression. **(c)** random forest regression. **(d)** new model.

Figure 6 (a-c) are the surface roughness images of the Kaufbeuren test site generated using the support vector regression, ANN regression and random forest regression, respectively. By comparing the above three images with

the surface roughness image generated using the new model (**Figure 6 (d)**), it can be understood that the surface roughness images generated by the machine learning-based regression models are matching with the surface roughness image generated by the new semi-empirical model.

Table 4 Comparison of the overall RMSE obtained by different models at the ground truth spots

Models	Dubois	New model	Multi dataset avg	ANN	Support vector	Random forest
RMSE (mm)	0.65	0.37	0.29	0.41	0.41	0.43

The RMSE values shown in **Table 4** are calculated between the model estimated h_{rms} and $GT\ h_{rms}$. From **Table 4**, it can be understood that the RMSE obtained by the new model is much lower (0.37 mm) compared to the Dubois model (0.65 mm). The RMSE can be further improved by performing the multi-dataset averaging technique (0.29 mm). The RMSE obtained by the machine learning-based models are almost the same (0.41 to 0.43 mm) and are only slightly higher compared to the new model RMSE (0.37 mm).

5 Conclusion

This study proposes the use of high-resolution airborne polarimetric SAR datasets for road surface roughness estimation. The X-band F-SAR datasets used in this study show very good sensitivity to the changes on the road surface and have the potential to remotely estimate the road surface roughness on a wide scale. The results obtained from the Dubois model shows that the model is biased due to its dependency on incidence angle variations and also due to its lower sensitivity at near range. A new semi-empirical model is proposed in this study for the HH and VV polarizations based on the assumptions from the Dubois model. The road surface roughness results obtained from the new model show a very good correlation with ground truth surface roughness data. Upper sigma nought threshold masking and lower SNR threshold masking were implemented to eliminate unreliable surface roughness values. Finally, the surface roughness images were generated only for the road surfaces and visualized in Google Earth with the help of the road layers from the Open Street Map (OSM). Multi-dataset averaging technique can be used to generate surface roughness images with fewer local variations. The initial surface roughness results obtained using the machine learning-based models are matching with the new model results and show good potential for further research. In the next phase of this study, further experiments are planned using an airborne polarimetric Ka-band SAR which, due to the smaller wavelength, will be more sensitive to the surface roughness differences. It is also planned to test the applicability of the new model on spaceborne SAR data, especially on high-resolution starring spotlight data acquired with TerraSAR-X and/or TanDEM-X.

References

[1] C. Y. Chan, B. Huang, X. Yan, and S. Richards, "Investigating effects of asphalt pavement conditions on traffic accidents in Tennessee based on the pavement management system (PMS)," *J. Adv. Transp.*, vol. 44, no. 3, pp. 150–161, 2010.

[2] R. Ghandour, A. Victorino, M. Doumiati, and A. Charara, "Tire/road friction coefficient estimation applied to road safety," in *18th Mediterranean Conference on Control and Automation, MED'10*, 2010, pp. 1485–1490.

[3] M.-T. Do and V. Cerezo, "Road surface texture and skid resistance," *Surf. Topogr. Metrol. Prop.*, vol. 3, no. 4, p. 43001, Oct. 2015.

[4] I. Hajnsek, "Inversion of Surface Parameters Using Polarimetric SAR," Friedrich Schiller University Jena, 2001.

[5] A. Babu and S. V Baumgartner, "Road Surface Roughness Estimation Using Polarimetric SAR Data," in *2020 21st International Radar Symposium (IRS)*, 2020, pp. 281–285.

[6] A. S. Yommy, R. Liu, Wu, and Shuang, "SAR Image Despeckling Using Refined Lee Filter," in *2015 7th International Conference on Intelligent Human-Machine Systems and Cybernetics*, 2015, vol. 2, pp. 260–265.

[7] I. Hajnsek, K. P. Papathanassiou, and S. R. Cloude, "Removal of additive noise in polarimetric eigenvalue processing," in *IGARSS 2001. Scanning the Present and Resolving the Future. Proceedings. IEEE 2001 International Geoscience and Remote Sensing Symposium (Cat. No.01CH37217)*, 2001, vol. 6, pp. 2778–2780 vol.6.

[8] M. Keller, J. Fischer, and M. Jager, "DLR's Airborne SAR F-SAR Product Description." Microwaves and Radar Institute, German Aerospace Center, Oberpfaffenhofen, 2019.

[9] P. C. Dubois, J. van Zyl, and T. Engman, "Measuring soil moisture with imaging radars," *IEEE Trans. Geosci. Remote Sens.*, vol. 33, no. 4, pp. 915–926, Jul. 1995.

[10] F. Ulaby *et al.*, *Microwave Radar and Radiometric Remote Sensing*. 2014.

[11] N. Baghdadi *et al.*, "A new empirical model for radar scattering from bare soil surfaces," *Remote Sens.*, vol. 8, no. 11, pp. 1–14, 2016.

[12] A. Singh, K. Gaurav, A. K. Rai, and Z. Beg, "Machine learning to estimate surface roughness from satellite images," *Remote Sens.*, vol. 13, no. 19, pp. 1–27, 2021.

[13] P. Mooney and M. Minghini, "A Review of OpenStreetMap Data," in *Mapping and the Citizen Sensor*, Ubiquity Press, 2017, pp. 37–60.